Sulfonated dopant-free hole-transport material promotes interfacial charge transfer dynamics for highly stable perovskite solar cells

Rui Li, Maning Liu, Sri Kasi Matta, Arto Hiltunen, Zhifeng Deng, Cheng Wang, Zhicheng Dai, Salvy P. Russo, Paola Vivo,* and Haichang Zhang**

R. Li, C. Wang, Z. Dai, Prof. H. Zhang,
Key Laboratory of Rubber-Plastics of Ministry of Education/Shandong Province (QUST), School of Polymer Science and Engineering, Qingdao University of Science and Technology, 53-Zhengzhou Road, Qingdao 266042, P. R. China
E-mail: haichangzhang@hotmail.com

Dr. M. Liu, Dr. A. Hiltunen, Prof. P. Vivo,
Hybrid Solar Cells, Faculty of Engineering and Natural Sciences, Tampere University, P.O. Box 541, FI-33014 Tampere University, Finland
E-mail: maning.liu@tuni.fi; paola.vivo@tuni.fi

Dr. Sri. Kasi Matta, Prof. Salvy. P. Russo,
Australian Research Council Centre of Excellence in Exciton Science,
School of Science, RMIT University, Melbourne, Victoria, Australia

Dr. Z. Deng
National and Local Joint Engineering Laboratory for Slag Comprehensive Utilization and Environmental Technology, School of Material Science and Engineering, Shaanxi University of Technology (SNUT), Hanzhong 723001, PR China

Keywords: interfacial modification, Pb-S bond, hole-transport material, perovskite solar cells, charge transfer dynamics, stability.

Abstract: The integration of a functional group into dopant-free hole-transport materials (HTMs) to modify the perovskite|HTM interface has become a promising strategy for high-performance and stable perovskite solar cells (PSCs). In this work, we report a sulfonated phenothiazine-based HTM, namely TAS, which consists of a butterfly structure with a readily synthesized *N*,*N*-bis[4-(methylthio)phenyl]aniline side functional group. The interaction

between TAS and perovskite via Pb-S bond induces a dipole moment that deepens the valence band of perovskite and thereby leads to enhanced open-circuit voltage in corresponding *n-i-p* PSCs. More importantly, the functionalization of perovskite surface via Pb-S bond promotes the hole extraction reaction while suppressing the interfacial non-radiative recombination, contributing to a 20–50% performance improvement compared to less- (4-(methylthio)-*N*-[4-(methylthio)phenyl]aniline, DAS) or non-interacting (*N*,*N*-bis(4-methoxyphenyl)aniline, TAO) counterparts. Consequently, TAS-based PSCs exhibit superior device stability with a high PCE retention (>90% of the initial value) after 125 days of storage in the air.

1. Introduction

Metal halide perovskite solar cells (PSCs) have become the forefront of next-generation photovoltaic research and have shown unprecedented achievements.[1–3] Very recently, an extremely high power conversion efficiency (PCE) of 25.6%, with a certified value of 25.2%, has been achieved by Jeong *et al.* for so-called α-$FAPbI_3$-based PSCs with a conventional *n-i-p* structure.[4] Since metal halide perovskites feature inherent outstanding optoelectronic properties, more and more research attention has been paid to the interfacial engineering between the perovskite layer and charge selective layers in PSCs,[5,6] aiming at functionalizing the perovskite surface for enhanced device performance and stability.

In a typical *n-i-p* PSC structure, a perovskite layer is capped with a hole-transport material (HTM), which extracts the holes from the valence band (VB) of perovskite while also protecting the perovskite surface. It is well known that metal halide perovskites present micrometer-scale photo-excited charge carrier diffusion lengths,[7] therefore, the losses of charge transport within the perovskites are minor. In other words, the major losses come from the charge recombination at the interfaces between the perovskite and the charge selective layers, e.g. perovskite|HTM. Numerous reports have been focusing on the optimization of interfacial engineering by

introducing a functional interlayer at the perovskite interfaces in PSCs.[5,6,8] In particular, a strong interfacial dipole moment is a proven promising tool to modify the interfaces via surface passivation. Lin *et al.* first created an interfacial dipole moment by depositing an ultrathin layer of tris(2,4,6-trimethyl-3-(pyridine-3-yl)phenyl) borane between a perovskite layer and ETM, favoring a swift electron extraction and hindering the interfacial charge recombination.[9] Cheng *et al.* employed a similar strategy to modify the interface of perovskite|HTM with *para*-substituted benzenethiol molecules, producing different dipole moments via an interaction between a donated lone pair at the sulfur atom and under-coordinated Pb^{2+} ions, namely Pb-S bond.[10] Abate *et al.* reported an interfacial self-assembled monolayer (SAM) with small molecules of amyl sulfide as a Lewis base, generating a negative dipole moment when the SAM binds to the Pb^{2+} ions of the perovskite surface.[11] Recently, the integration of various functional groups in the dopant-free HTMs,[12,13] e.g. sulfur- and oxygen-containing side chains, has fueled a rising research interest in interfacial engineering since it enables the simultaneous functionalization of the perovskite surface and the selective hole transfer. Combining two functions in one molecule removes an extra interface in the device and promotes a simple fabrication process. Chen *et al.* calculated the binding energy of the Pb-S bond between a methylsulfonyl group-based HTM (TPP-SMeTAD) and $CH_3NH_3PbI_3$ ($MAPbI_3$) perovskite. This bond was stronger than the Pb-O bond formed between the same perovskite and a similar HTM with oxygen atom as the terminal substituent (TPP-OMeTAD).[14] The authors found that the TPP-SMeTAD-based devices exhibit both enhanced performance and reduced hysteresis in *p-i-n* PSCs over the devices employing TPP-OMeTAD. Later on, Yin *et al.* reported the replacement of an O atom with S atom in the terminal of a dopant-free HTM to generate the Pb…S interaction, which enhances the stability and performance of PSCs.[15] However, a deep understanding of how the dipole moment induced by the Pb-S coordination bond affects the inherent properties of perovskite and on the charge transfer dynamics at the perovskite and sulfonated dopant-free HTM interface is still lacking.

Phenothiazine (PTZ), as an electron-rich unit, contains nitrogen and sulfur atoms in the middle core with two active sites at the 3 and 6 positions, which enables further chemical modifications. The PTZ core with a butterfly structure allows the substitution of the end functional groups, which has been employed as a promising strategy in HTM designs for PSCs.[16,17] In this work, we first constructed a PTZ-based small molecule by introducing substituted *N*,*N*-bis[4-(methylthio)phenyl]aniline (denoted as TPA-SCH_3) electron-rich functional group on each side, namely TAS. As a comparison, two reference small molecules were also designed by replacing the functional group of TPA-SCH_3 with *N*,*N*-bis(4-methoxyphenyl)aniline (TPA-OCH_3) and 4-(methylthio)-*N*-[4-(methylthio)phenyl]aniline (DPA-SCH_3), i.e. TAO and DAS, respectively (see **Scheme 1**). In a TAS molecule, the well-matched D-D-D (donor-donor-donor) alignment provides a highly planar molecular backbone and extended π-conjugation, which favor the efficient hole transfer within the individual molecule as well as between the adjacent molecules.[18] In addition, the sulfur atom contained in the functional group can modify the perovskite surface via dipole intermolecular interaction between a lone pair and Pb^{2+}, when TAS is used as a dopant-free HTM in *n-i-p* PSCs. Based on our theoretical and experimental results, TAS exhibits remarkably enhanced hole extraction, hole transport, and device performance compared to TAO and DAS. More importantly, the dipole moment induced by the interfacial Pb-S bond can deepen the perovskite valence band, leading to an enhanced open-circuit voltage (V_{oc}) in PSCs. Such interfacial modification via Pb-S bond without the introduction of an interlayer in TAS-based PSCs can also promote superior device stability with extremely high PCE retention (>90%) after 125 days of shelf storage under ambient conditions (in darkness, RH~40%).

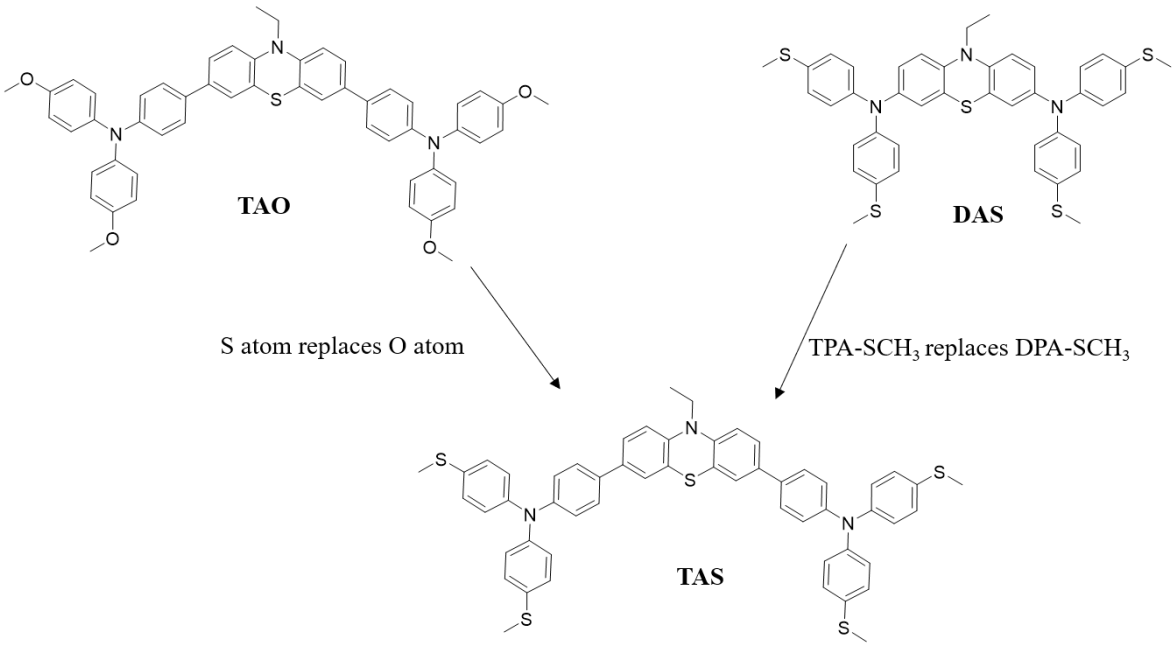

Scheme 1. Chemical structures of TAO, DAS, and TAS.

2. Results and discussion

TAS and TAO were synthesized through Suzuki reaction between PTZ and TPA-SCH_3 or TPA-OCH_3, while DAS was obtained by Buchwald reaction between the PTZ and DPA-SCH_3, respectively, with a yield of up to 77 %. The synthetic routes are described in detail in the Supporting Information (SI) and the products were characterized by ^{1}H and ^{13}C NMR and mass spectroscopies (**Figure S1**-**S13**). All the molecules show high thermal stability with 5 % weight loss at 384–410 °C (**Figure S14**). The synthetic costs of PTZ-HTMs are low and estimated to be \$14.03/g (DAS), \$20.57/g (TAO), and \$51.94/g (TAS) (see the detailed cost analysis in **Table S1**-**S10** in SI) according to previously reported calculation methods,[15,19,20] which are much cheaper than the commercially common HTMs, e.g. Spiro-OMeTAD (\$91.67/g) and PTAA (\$423.3/g).[21,22]

2.1. Optical, electrochemical, and hole-transporting properties of PTZ-HTMs

Figure 1a and 1b show the absorption spectra of PTZ-HTMs in solution and film, respectively. All the molecules exhibit their first exciton peaks in the UV range of 328–384 nm (**Table 1**). The absorption bands of PTZ-HTMs in the range of 250–300 nm can be assigned to the n-π* transition of the phenylamine moieties.[23] All PTZ-HTMs represent red-shifted exciton peaks in film state accompanied with an absorption tail in the long wavelength region (500–600 nm) compared to their solution phase, indicative of aggregation and close stacking occurring in the thin film. Interestingly, a relatively larger red shift in-between solution and film phase is observed for the absorption spectra of TAS (18 nm) and TAO (34 nm) compared to that of DAS case (7 nm). This implies that an additional benzene ring in the functional group (e.g. TAS or TAO) can lead to the molecular backbone in high planarity structures, which typically induces the aggregation. In addition, TAO exhibits a large bathochromic shift compared to DAS and TAS, possibly ascribed to the significantly smaller size of the oxygen atom of TAO compared to that of the sulfur atom of DAS or TAS. This, in turn, enables a stronger aggregation for TAO-HTM in the film state. We estimated the optical bandgaps as 3.08 eV (DAS), 2.92 eV (TAS), and 2.88 eV (TAO) based on their corresponding absorption onsets (see Table 1).

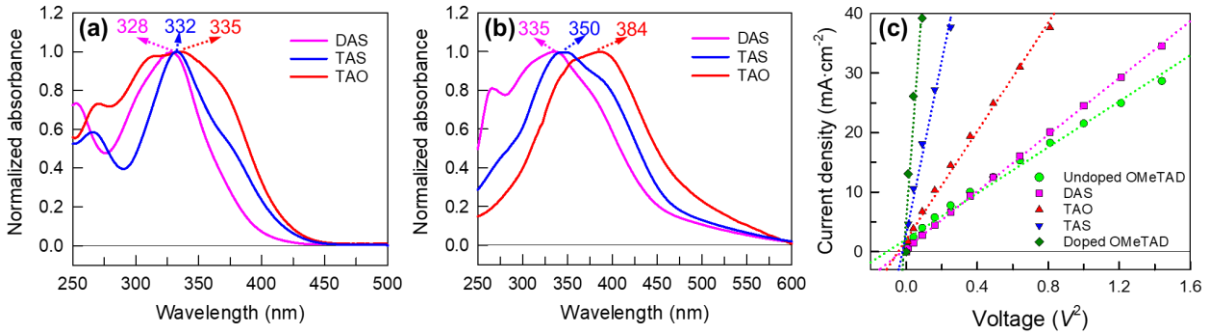

Figure 1. Normalized absorption spectra of PTZ-HTMs (a) in chloroform solution and (b) in film state. (c) Dark current density (J)–voltage (V^2) curves of hole-only devices with structure 'ITO/PEDOT:PSS/HTM/MoO_3/Au' for different HTMs including undoped and doped Spiro-OMeTAD (denoted as OMeTAD) as the references. Dotted lines show the fitting results with a linear function.

Suitable frontier molecular orbital energy levels of HTMs are paramount for optimum energy alignment in PSCs. The electrochemical properties of PTZ-HTMs were studied by conducting cyclic voltammetry (CV) measurements (See **Figure S15**). From the onsets of anodic oxidation, the HOMO levels were estimated as -4.94 eV, -5.12 eV, and -5.16 eV *vs.* vacuum level for DAS, TAO, and TAS, respectively. The deep HOMO levels of PTZ-HTMs can be attributed to the strong electron donor character of the composited groups such as PTZ core and phenyl-aniline. Compared to the HOMO level (-5.04 eV) of a reference Spiro-OMeTAD measured under the same conditions, our synthesized PTZ-HTMs show favorable energy level alignment, providing sufficient driving force for the hole extraction from perovskite to the HTMs.[24] The LUMO levels of PTZ-HTMs were then calculated according from the estimated optical bandgaps (see Table 1).

To further evaluate the suitability of these PTZ-HTMs for PSC applications, we measured their hole mobilities by employing the space-charge-limited current (SCLC) technique (see more details in SI). Figure 1c depicts the comparison of dark $J–V^2$ curves of the hole-only devices with different HTMs, and their hole mobilities were extracted based on **Equation S3** and are summarized in Table 1. Among all three dopant-free PTZ-HTMs, TAS has the highest hole mobility (6.1×10^{-4} cm^2 V^{-1} s^{-1}), which is nearly two times and seven times higher than that of TAO (3.2×10^{-4} cm^2 V^{-1} s^{-1}) and DAS (9.1×10^{-5} cm^2 V^{-1} s^{-1}), respectively. The higher mobility of TAS (6.1×10^{-4} cm^2 V^{-1} s^{-1}) compared to DAS (9.1×10^{-5} cm^2 V^{-1} s^{-1}) can be explained by two possible reasons: *(i)* In TAS there is an additional benzene ring between the PTZ core and the end group with respect to DAS, which results in π-extension and guarantees more planar backbone for TAS. This is beneficial for the hole transfer within the molecule. *(ii)* As shown in the Figure 1a and 1b, there is an 18 nm bathochromic shift in the absorption spectra of TAS when comparing its solution and film phase, while a red shift of only 7 nm is observed for DAS. This indicates that a stronger aggregation occurs in the case of TAS compared to DAS, which is favorable for the hole transport between the neighboring molecules. Moreover, two additional

causes could be highlighted to explain the improved hole mobility (6.1×10^{-4} cm^2 V^{-1} s^{-1}) of TAS *vs.* TAO (3.2×10^{-4} cm^2 V^{-1} s^{-1}): *(i)* Both end groups of TAS are TPA-SCH_3, while those of TAO are TPA-OCH_3. Since TPA-SCH_3 exhibits a stronger donor ability compared to TPA-OCH_3, the former group leads to an enhanced donor-donor interaction in the TAS molecule compared to TAO, which is beneficial for the charge transfer within a single molecule. *(ii)* Our previous study also indicates that the thionation reaction could improve the hole mobility of dopant-free HTM molecules upon the replacement of an O atom with S atom.[25] It is noteworthy that dopant-free TAS nearly shows a hole mobility (6.1×10^{-4} cm^2 V^{-1} s^{-1}) as high as that of doped Spiro-OMeTAD (7.2×10^{-4} cm^2 V^{-1} s^{-1}) measured under identical conditions, suggesting that TAS can act as an efficient hole-transport material without a doping requirement in the fabrication of PSCs.

Table 1. Optical, electrochemical, and hole-transporting properties of dopant-free PTZ-HTMs.

HTM	$\lambda_{abs,max}$ (nm)		HOMO[a] (eV)	LUMO[b] (eV)	E_g^{opt}[c] (eV)	μ_h[d] (cm^2 V^{-1} s^{-1})
	in solution	in film				
DAS	328	335	-4.94	-1.86	3.08	9.1×10^{-5}
TAO	335	384	-5.12	-2.24	2.88	3.2×10^{-4}
TAS	332	350	-5.16	-2.24	2.92	6.1×10^{-4}

[a]HOMO level was obtained by CV measurement: $-E_{HOMO} = E_{onset(ox)} + 4.8$ eV, where $E_{onset(ox)}$ is the onset potential for the oxidation vs. ferrocene.; [b]LUMO level was obtained from the equation of $E_{LUMO} = E_{HOMO} + E_g^{opt}$; [c]Optical band gap E_g^{opt} was determined at the absorption onset of the material in solution phase ($E_g^{opt} = 1240 / \lambda_{abs,onset}$ eV); [d]Hole mobility.

2.2. Computed Pb-S bond at the interface of perovskite and PTZ-HTMs

The adsorption state of each PTZ-HTM on the surface of the $MAPbI_3$ perovskite, which was used in this study as a prototype of the actual triple-cation halide perovskite, was investigated by DFT simulations (see the detailed computational methods in SI). The adsorption of PTZ-HTMs was modeled on PbI_2-terminated (001) surfaces of perovskite slabs in two interaction orientations, i.e. vertically and parallelly oriented HTM molecules, in order to investigate the

formation of Pb-S (for TAS and DAS) or Pb-O bonds (for TAO) at the interface of the perovskite and HTMs.

Figure 2 shows the optimal adsorption structures of PTZ-HTMs on the perovskite slab surface with the HTMs in a vertical orientation (for the parallel orientation see **Figure S16**a-c). Regardless of the interaction orientation, TAS and DAS adsorb closer to the perovskite surface accompanied with higher adsorption energies than those obtained in the case of TAO, as determined by comparing the bond length and adsorption binding energies for Pb-S and Pb-O (see **Table S11**). This suggests that the sulfur-containing functional group (i.e. TAS or DAS) can anchor to the perovskite via a Pb-S bond in a uniform and intact distribution while the oxygen-containing functional unit (i.e. TAO) shows some random anchoring to the perovskite surface with insufficient adsorption. Our results are consistent with a previously reported DFT study on the adsorption of diverse tert-butyl benzene (tB)-based functional moieties on perovskite surfaces.[26] That study estimated the absolute adsorption energies of tB-SH (-0.57 eV) and tB-OCH_3 (-0.48 eV), demonstrating that the lone electron pairs of sulfur can occupy the empty 6*p* orbitals of Pb^{2+} leading to a stronger Pb-S coordination bond compared with the Pb-O bond. Interestingly, in the vertical orientation TAS exhibits a consistent enhancement in adsorption energy (-3.24 meV/Å^2) and shorter bond-length (3.39 Å) compared with that of DAS (-3.11 meV/Å^2 and 3.55 Å respectively). In addition, both the interaction angles of TAS-PbI_2 (S-Pb-I, 87.3°) and TAO-PbI_2 (O-Pb-I, 91.1°) are much larger than that of DAS-PbI_2 (S-Pb-I, 59.1°). Such a big difference is mainly caused by the additional benzene ring inserted between the PTZ core and the end group of TAS or TAO compared to DAS, which results in a more flexible backbone and, thus, a wider range of interaction angles. This trend has been observed for both vertical and parallel orientations based on our DFT calculations (see Table S11).

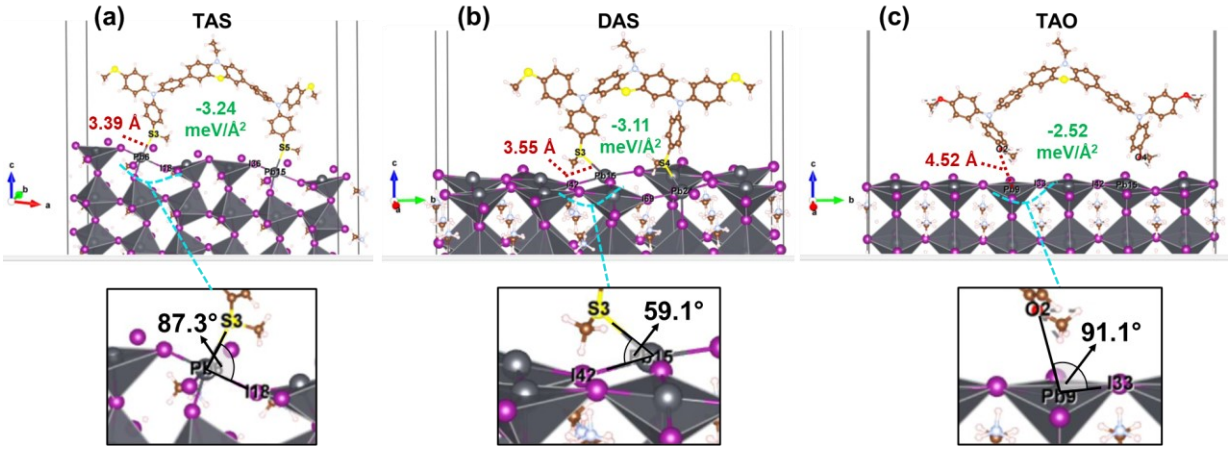

Figure 2. Calculated optimized adsorption structures of (a) TAS, (b) DAS, and (c) TAO on the PbI_2-terminated surface of $CH_3NH_3PbI_3$ (i.e. $MAPbI_3$) perovskite in a vertical orientation. Corresponding adsorption energies (in meV/Å^2) and Pb-S or Pb-O bond lengths (in Å) are highlighted in green and red colors, respectively. Amplified absorption states are shown in bottom black boxes, marked with the interaction angles of S-Pb-I for (a) and (b), and O-Pb-I for (c).

To further assess the interatomic charge redistribution for the systems, we have evaluated the space charge density dispersion at the perovskite|PTZ-HTM interfaces in both vertical and parallel orientations (**Figure S17**). In the case of vertical aligned HTMs-perovskite systems, the vertical TAS-PbI_2 has relatively more charge accumulation in the sulfur region of the Pb-S bond. The charge depletion region at the Pb atom of the Pb-S bond is relatively small. This suggests that hole transfer could be more favorable in TAS compared with TAO-PbI_2. The DAS-PbI_2 system has a similar charge accumulation region at the sulfur atom as that of TAS-PbI_2, but the depletion region at Pb in the S-Pb bond is greater compared with TAS-PbI_2. Thus, hole transport is relatively more constrained in DAS compared with TAS. Based on the same logic, however, the DAS system might have a higher hole transfer amplitude than TAO. The systems that have parallelly aligned HTMs on the perovskite surface have also shown similar charge density distributions at the HTM-perovskite bonding interface like those of vertically aligned systems and, hence, are predicted to have a similar order of hole transfer feasibility.

It is noteworthy that the work function of the perovskite, which was obtained from the DFT calculations (Table S11), increases when moving from DAS (5.05 eV) to TAO (5.40 eV) to

TAS (5.54 eV) in the vertical orientation, likely due to the energy change induced by the inherent dipole of the molecule with higher planarity, i.e. TAO and TAS (see Figure S16d-f).[27] More importantly, the increase in work function can effectively deepen the valence band of the perovskite,[11] and consequently can improve V_{oc} in PSCs, which we have indeed observed, as will be discussed in detail in Section 2.5. Based on our simulation results, the strong adsorption of TAS via the Pb-S bond formed on the perovskite surface is expected to not only promote interfacial charge transfer dynamics (e.g. hole extraction) but also prevent the penetration of water/oxygen into the perovskite layer, thus enhancing the device stability. Both aspects will be experimentally validated in the following sections.

2.3. Influence of Pb-S bond on interfacial charge transfer dynamics

To clarify the influence of the Pb-S bond on the interfacial hole extraction process, we first compared the steady-state photoluminescence (PL) spectra of glass/CsFAMA/PTZ-HTMs with that of glass/CsFAMA as the reference in **Figure 3**a, where CsFAMA stands for a triple-cation perovskite (see the full stoichiometry in SI). A clearly enhanced PL quenching was observed by coating either TAS or DAS layer on the perovskite film compared to the case of TAO layer. The calculated quenching efficiencies, i.e. hole extraction efficiencies, are 92.1%, 97.4%, and 99.1% for TAO, DAS, and TAS, respectively. This suggests that the Pb-S bond formed at the interface of perovskite and sulfur-containing HTM (TAS or DAS) can effectively promote the interfacial charge separation, i.e. hole extraction process. The hole extraction dynamics were also observed by comparing the time-resolved PL (TRPL) decays in Figure 3b. A clear decay acceleration was detected for both glass/CsFAMA/TAS and glass/CsFAMA/DAS compared to glass/CsFAMA/TAO, confirming that the hole at the perovskite/HTM interface can be swiftly extracted with the help of the Pb-S bond.

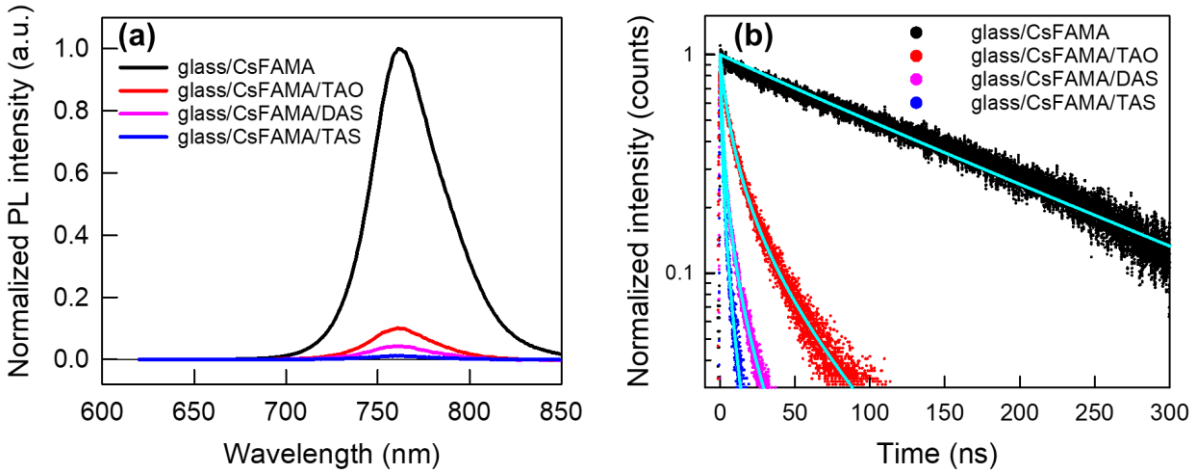

Figure 3. (a) Steady-state photoluminescence (PL) spectra (excited at 600 nm) and (b) time-resolved PL (TRPL) decays (excited at 483 nm and monitored at 755 nm) of glass/CsFAMA and glass/CsFAMA/HTM with various PTZ-based HTMs. Solid lines show the fitting results with a rate law function.

We then attempted to quantitatively analyze the PL decay data by employing a kinetic model, namely the one-dimension charge diffusion model (see the detail analysis method in SI).[28] Since the charge diffusion is ultra-fast within the perovskite layer, the overall charge extraction process is limited by the interfacial charge transfer. This model was previously reported to explain the transient emission decay data for $MAPbI_3$ perovskite coated on charge acceptors (e.g. TiO_2 or Spiro-OMeTAD).[29] A rate equation (see **Equation S4** in SI) was here used to quantify the PL decay data for glass/CsFAMA/HTMs samples, including first-order recombination via carrier trap sates, second order non-geminate free charge carrier (electron and hole) recombination, and interfacial charge transfer process (i.e. hole extraction). A simplified equation (see **Equation S6**) was employed to describe the perovskite excited state dynamics with only two components (first and second order recombination). The fitted results, obtained by solving **Equations S5** and **S7**, are presented as a solid line in Figure 3b, suggesting that this kinetic model fits the data well. For the perovskite excited-state decay (glass/CsFAMA), the second-order component dominates the fitting of the decay data upon an excitation intensity of > 20 nJ cm^{-2} (~30 nJ cm^{-2} in our case), indicating that two-carrier recombination takes place

within the perovskite layer.[30] Our global analysis extracted first-order (k_1) and second-order (k_2) rate constants as 6.4×10^{6} s^{-1} and 3.3×10^{-10} s^{-1} cm^3, respectively. This rate constant of second-order recombination is as high as those reported for $MAPbI_3$ and $FAPbI_3$ perovskite films,[31] and it is attributed to the direct allowed inter-band optical transition. On the other hand, the interfacial hole extraction process dominates to fit the decay data for glass/CsFAMA/HTMs samples. The resulting k_1, k_2, and k_{HT} (i.e. hole extraction rate constant) for each of the PTZ-based HTM are summarized in **Table 2**. Interestingly, the first-order (k_1) rate constant decreases from 1.1×10^{8} s^{-1} (TAO) to 3.7×10^{7} s^{-1} (DAS) to 1.7×10^{7} s^{-1} (TAS), while the hole extraction rate constant (k_{HT}) increases correspondingly from 9.5×10^{7} s^{-1} cm^3 (TAO) to 3.8×10^{8} s^{-1} cm^3 (DAS) to 6.6×10^{8} s^{-1} cm^3 (TAS). This suggests that the interfacial Pb-S bond not only promotes the hole extraction but also hinders the single-carrier trapping recombination by effectively filling the surface traps of the perovskite. It is noted that the second-order (k_2) rate constants for the cases of all three HTMs are similar to that of pure CsFAMA perovskite, indicating that the hole extraction process does not influence the non-geminate electron-hole recombination within the perovskite layer. To quantify the hole trap density on the perovskite surface, we fabricated hole-only devices with structure 'ITO/PEDOT:PSS/perovskite/HTM/MoO_3/Au'.[32,33] The dark *J–V* curves were measured for these devices, as shown in **Figure S18**. By following **Equation S12**, we calculated the hole trap densities of the perovskite films with different PTZ-HTMs as 4.48×10^{15} cm^{-3} (TAS), 6.03×10^{15} cm^{-3} (DAS), and 1.20×10^{16} cm^{-3} (TAO). This clearly reveals that the Pb-S coordination bond at the perovskite/HTM (TAS or DAS) interface can effectively reduce the trap density compared to the case of TAO. TAS exhibits further suppressed trap density compared to that of DAS due to the formation of a stronger Pb-S bond at the interface, which has been proved by previous DFT calculation results (Table S11). The deviation trend of the trap density among the three PTZ-HTMs is highly consistent with the fitted k_1 (the rate constant of trap state mediated recombination) from TRPL decay data (Table 2).

Since the PL decays comprise either two (glass/CsFAMA) or three (glass/CsFAMA/HTMs) components, it is not easy to assess the lifetime. We thus defined an effective lifetime, $\tau_{1/e}$, expressed as **Equation S8** in SI. The effective lifetime of the excited state decay (glass/CsFAMA) was estimated as 142.5 ns, similar to the previous report.[34] Those effective lifetimes of the PL decays for glass/CsFAMA/HTMs were determined and are summarized in Table 1, confirming the fastest hole extraction rate ($\tau_{1/e}$ = 1.5 ns) at the interface of CsFAMA/TAS and the slowest one ($\tau_{1/e}$ = 9.8 ns) for TAO without interfacial Pb-S bond. The accelerated hole extraction rate in the case of TAS compared to that ($\tau_{1/e}$ = 2.6 ns) of DAS is ascribed to the enhanced Pb-S binding energy (-3.24 eV) of TAS compared to that (-3.11 eV) of DAS, as described in previous simulation results (Table S11). Following these data, the hole extraction efficiencies were estimated as 93.2%, 98.1%, and 99.2% for TAO, DAS, and TAS (see Table 2), respectively, using **Equation S11** that is derived from **Equation S9** and **S10**. The estimated hole extraction efficiencies are highly consistent with those calculated from the PL quenching data, implying that the kinetic model indeed agrees well with the PL decay data.

Table 2. Photophysical properties of PTZ-HTMs.

HTM	k_1 (s^{-1})	k_2 (s^{-1} cm^3)	k_{HT} (s^{-1})	$\tau_{1/e}$ [a] (ns)	$\emptyset_{ext}$ [b] (%)
TAO	1.1×10^8	3.7×10^{-10}	9.5×10^7	9.8	93.2
DAS	3.7×10^7	3.4×10^{-10}	3.8×10^8	2.6	98.1
TAS	1.7×10^7	3.6×10^{-10}	6.6×10^8	1.5	99.2

[a]Effective lifetime; [b]Hole extraction efficiency.

2.4. Performance of PTZ-HTMs-based perovskite solar cells

The previous CV data (Section 2.1) have confirmed the suitability of the HOMO levels of PTZ-based small molecules for a good energy level alignment with the VB of CsFAMA perovskite. **Figure 4**a shows the energy level diagram of the standard mesoporous *n-i-p* PSCs using DAS, TAO, and TAS as HTMs. The complete PSC structure is FTO/c-TiO_2/m-TiO_2/CsFAMA/PTZ-HTM/Au (see the fabrication details in SI), as illustrated in the cross-sectional SEM image (Figure 4b). Note that in this work a relatively large active area (i.e. 36

mm^2, see the inset photo in Figure 4c) was employed to clarify the effect of new dopant-free PTZ-HTMs on the device performance including the stability on a relatively large scale. We first optimized the concentration of PTZ-HTMs in chlorobenzene solution by using TAS as an example, aiming at the best PCE. **Table S12** presents the comparison of champion device performance with different TAS concentrations (5–20 mg/mL), indicating that the best cell was achieved with a ~65 nm thick TAS layer (determined in Figure 4b) made from a concentration of 10 mg/mL. We note that the FF (0.58) of the best cell is still at a moderate level, plausibly due to the very thin dopant-free HTM layer which requires further molecular engineering to improve its charge conductivity in a thick layer (e.g. > 150 nm). We have indeed measured the conductivity of the three PTZ-HTMs. The highest (2.8×10^{-6} S cm^{-1}) value is achieved with the pristine TAS film (see **Figure S19** and **Table S13**). However, this is still one order of magnitude lower than the conductivity (> 3×10^{-5} S cm^{-1}) of doped Spiro-OMeTAD.[35] This concentration (10 mg/mL) was then applied for the other two PTZ-HTMs (DAS and TAO) for comparison upon an identical process. Figure 4c illustrates the comparison of current density (J)–voltage (V) of the champion devices based on three PTZ-HTMs, recorded under 1 Sun condition (AM 1.5G, 100 mW cm^{-2}) and under forward and reverse scans. **Table 3** summarizes the average device performance (12 cells for each case), together with the photovoltaic parameters of the champion cells. Compared to those derived from DAS (PCE of 6.8%) or TAO (PCE of 11.1%), the TAS-based PSCs show a significantly improved J_{sc} of 22.5 mA cm^{-2}, an enhanced V_{oc} of 1.04 V, and a higher PCE of 13.3%. It is worth noting that a maximum PCE of 14.1% was achieved by a champion dopant-free TAS-based device with an active area of 20 mm^2, which is much larger than that commonly reported (<10 mm^2) for highly efficient devices.[10] The increase in V_{oc} is surprisingly in good agreement with the simulated upward shift of perovskite work function (Table S11) in the case of vertically oriented HTM systems. This implies that the interaction between TAS and perovskite surface, i.e. Pb-S bond induced dipole moment, can deepen the VB of perovskite and induce an enhanced V_{oc} (>20 mV). In

addition, an obviously reduced hysteresis in the *J–V* curves of TAS-based devices (H-index = 1.21) is observed compared to other two cases (DAS: H-index = 1.47; TAO: H-index = 1.38), attributed to the swift hole transfer efficiently escaping from the perovskite|TAS interface after the hole extraction, and to the reduced built-in electric field at the interface.[36]

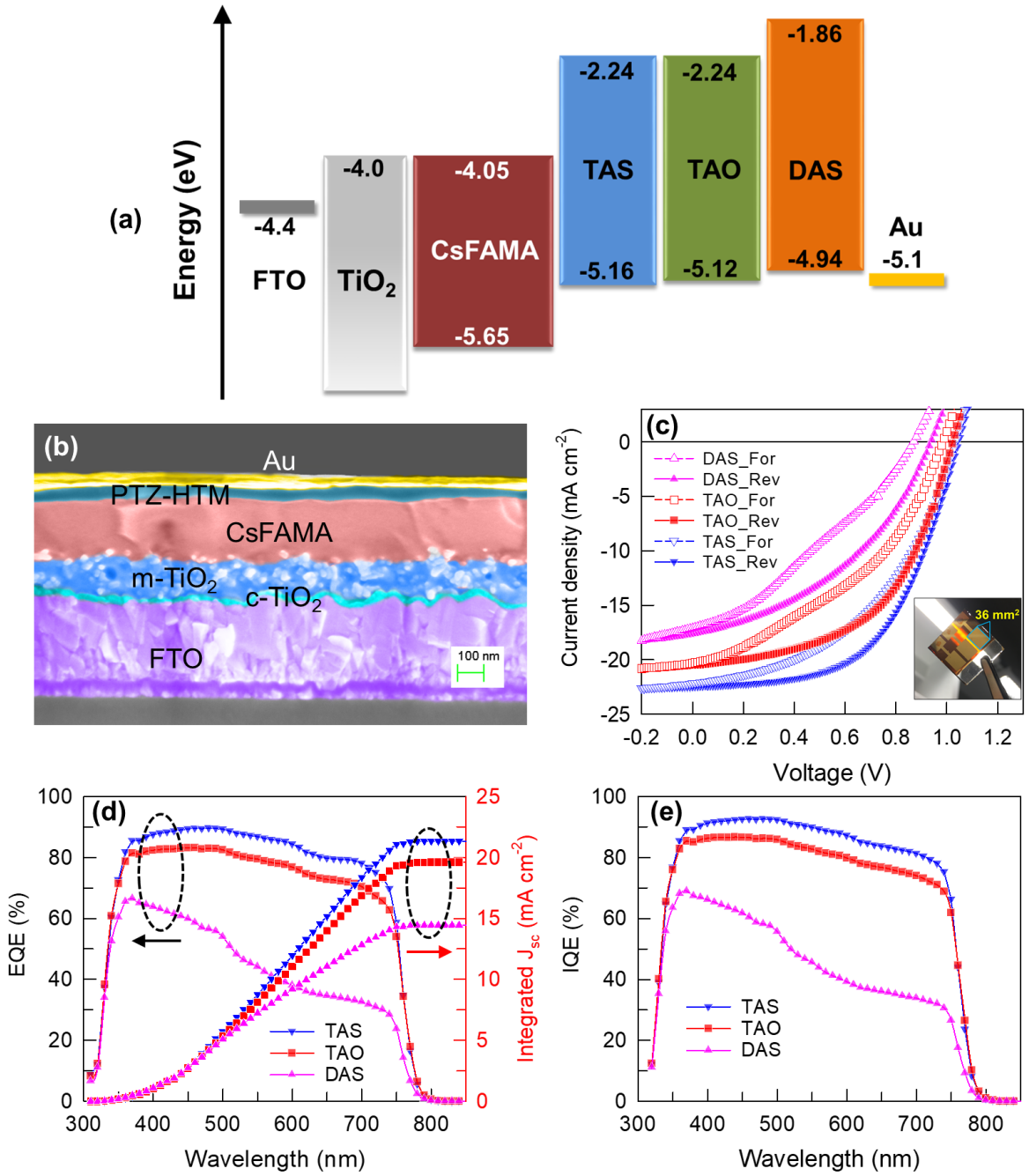

Figure 4. (a) Energy level diagram for PTZ-HTMs, and other layers of the CsFAMA-based solar cells in *n-i-p* structure. (b) Cross-sectional SEM image of a typical TAS-based perovskite solar cell (PSC), observed at 3 kV. (c) *J–V* curves of the champion PTZ-HTMs-based PSCs under 1 sun illumination (forward and reverse scans with a scan rate of 50 mV/s). (d) External

quantum efficiency (EQE) spectra and integrated J_{sc} values, and (e) Internal quantum efficiency (IQE) spectra of the champion PTZ-HTMs-based PSCs.

External quantum efficiency (EQE) spectra (Figure 4d) indicate that the interfacial charge separation dominates the photocurrent generation efficiency since all three PTZ-HTMs can achieve relatively high hole extraction efficiencies (> 90%). The integrated J_{sc} from EQE spectra shows less than 8% mismatch on average compared to that obtained from the *J–V* curves. Internal quantum efficiency (IQE) spectra (Figure 4e) were simultaneously measured by the same quantum efficiency setup, making a good agreement with the EQE data trend. Since it is known that the hole extraction process dominates the overall charge separation efficiency ($\emptyset_{\mathrm{sep}}$) in PSCs,[29,37] we can assume that the $\emptyset_{\mathrm{sep}}$ is nearly equal to the hole extraction efficiency ($\emptyset_{\mathrm{ext}}$), as shown in Table 2. We then calculated the charge collection efficiency ($\emptyset_{\mathrm{col}}$) based on Equation 1, as summarized in Table 3.

$$\emptyset_{\mathrm{col}} = \frac{\mathrm{IQE}}{\emptyset_{\mathrm{sep}}} = \frac{\mathrm{IQE}}{\emptyset_{\mathrm{ext}}} \quad (1)$$

The enhanced charge collection efficiencies of 93.3% and 92.8% in TAS- and TAO-based devices compared to DAS (70.2%) further confirms that the high planarity of molecular structure for TAS and TAO favors the hole transport within the HTM.

Table 3. Performance of perovskite solar cells with different PTZ-HTMs. All data for photovoltaic parameters are obtained from the reverse scan.

HTM	PCE (%)	J_{sc} (mA cm^{-2})	V_{oc} (V)	FF (%)	H-index[a)]	EQE_{max} (%)	IQE_{max} (%)	$\emptyset_{col}$ (%)
DAS	6.5±0.3 (6.8)[b)]	17.2±0.5 (17.7)	0.91±0.02 (0.93)	40.8±0.6 (41.4)	1.49±0.02 (1.47)	66.5	68.9	70.2
TAO	10.8±0.3 (11.1)	20.2±0.3 (20.5)	1.01±0.01 (1.02)	52.6±0.5 (53.1)	1.39±0.01 (1.38)	83.2	86.5	92.8
TAS	12.9±0.4 (13.3)	22.2±0.3 (22.5)	1.03±0.01 (1.04)	56.3±0.5 (56.8)	1.22±0.01 (1.21)	89.7	92.6	93.3

[a)]H-index is calculated as PCE_{rev}/PCE_{for}, where PCE_{rev} and PCE_{for} present PCEs measured under reverse and forward scans, respectively; [b)]The values in brackets represent the parameters of the champion cell.

2.5. Stability study

To directly identify the degradation processes taking place in perovskite films, we conducted long-term shelf lifetime measurements for the unencapsulated PTZ-HTMs-based devices by comparing them with reference doped Spiro-OMeTAD-based devices. All tested devices were stored in darkness under ~40% RH throughout the storage period. **Figure 5**a depicts the variation of the absolute PCEs as a function of the storage time for the champion cells with different HTMs. Although the initial PCE of the reference device with doped Spiro-OMeTAD was as high as 17.1%, it dropped below the PCE of TAS-based device after 37 days of storage. The PCE of TAS-based device was highly retained (>90%) after 125 days of storage under ambient conditions (see Figure 5b), which we believe represents one of the highest stabilities for reported dopant-free HTMs in *n-i-p* PSCs.[38,39] This clearly suggests that the Pb-S bond can be evenly formed covering the whole coating area (>36 mm^2 active area) and induce the formation of kinetic barriers at the interface that slow the penetration of H_2O and O_2 into the perovskite layer. This Pb-S bond protection effect was also observed for DAS-based devices as the PCE still retained over 80% of its peak value after about 100 days of storage, while the PCE of the TAO-based device dropped to below ~65% of the peak PCE over the same measurement period. Note that an initial PCE growth was observed for all cases, thus, we normalized the PCE decay curves with their respective peak values after stabilization, as shown in Figure 3b. The TAS-based device exhibits an extremely long predicted T_{80} lifetime[39] of 160 days while the doped Spiro-OMeTAD-based device experimentally represents a short T_{80} lifetime of ~26 days. Figure 5c and 5d compare the *J–V* curves of the stabilized (with maximum PCE) and aged devices after 125 days of storage for Spiro-OMeTAD reference and TAS cases, respectively. The PCE (12.0%) of the aged champion TAS-based cell displays a nearly 45% performance enhancement compared to that (6.8%) of the aged reference cell. This emphasizes that the dopant-free sulfur-containing small molecular HTMs (e.g. TAS in our work) could be a more favorable choice to replace the conventional doped Spiro-OMeTAD in PSCs, especially when considering practical applications requiring good long-term stability.

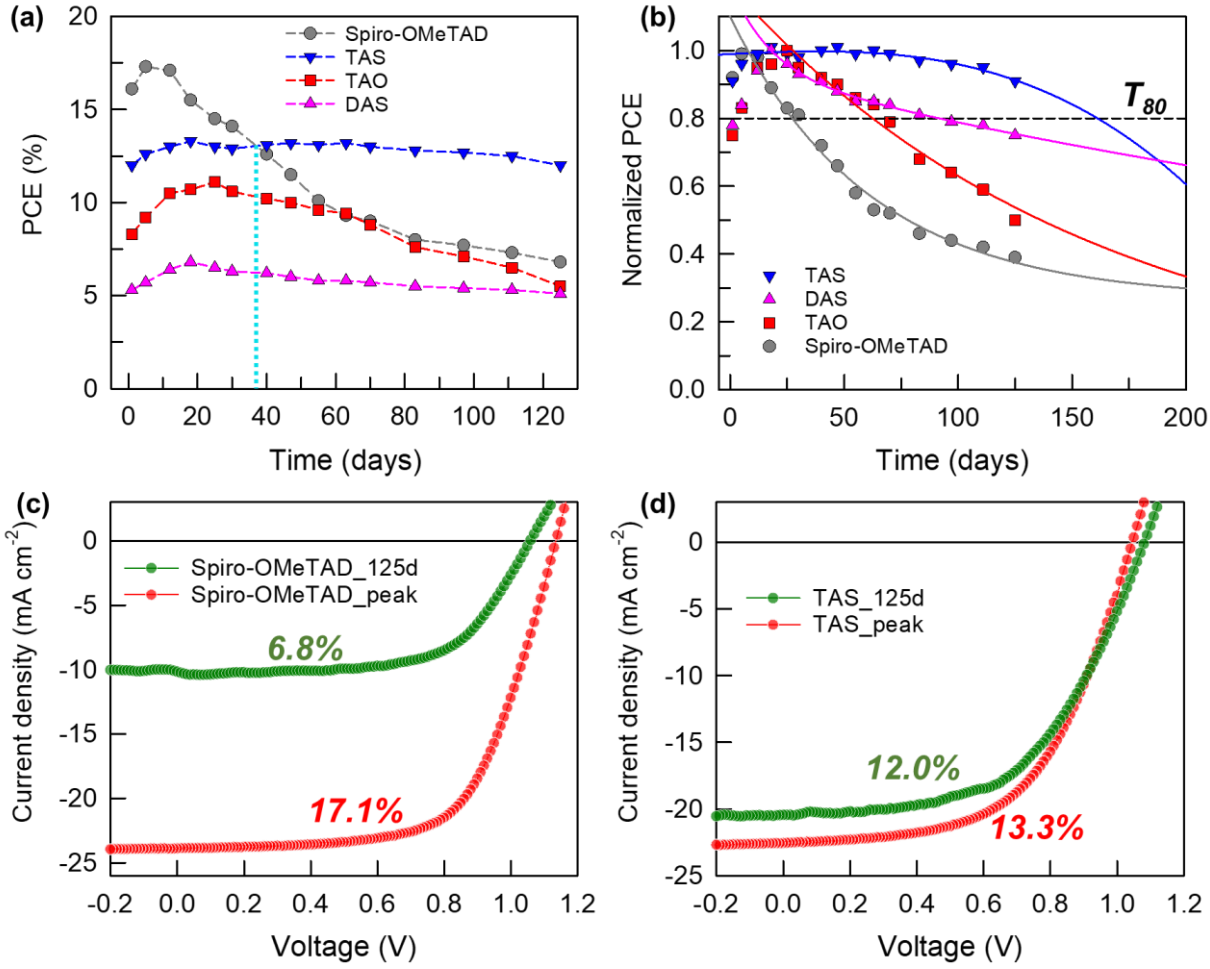

Figure 5. (a) PCE and (b) Normalized PCE of the champion PSCs with different HTMs vs. storage time, stored under ambient conditions (in darkness, RH~40%). Dotted line in (a) shows the time (about 37 days) when the absolute PCE of TAS-based device surpasses that of Spiro-OMeTAD-based reference device. Dash line in (a) is a guide to the eye. T_{80} in (b) represents the time when the PCE decreases to 80% of its maximum value. Solid line in (b) shows the decay curve after the maximum PCE is achieved. Comparison of *J–V* curves of stabilized (with peak PCE) and aged (125 days, 125d) devices with (c) reference doped Spiro-OMeTAD and (d) TAS.

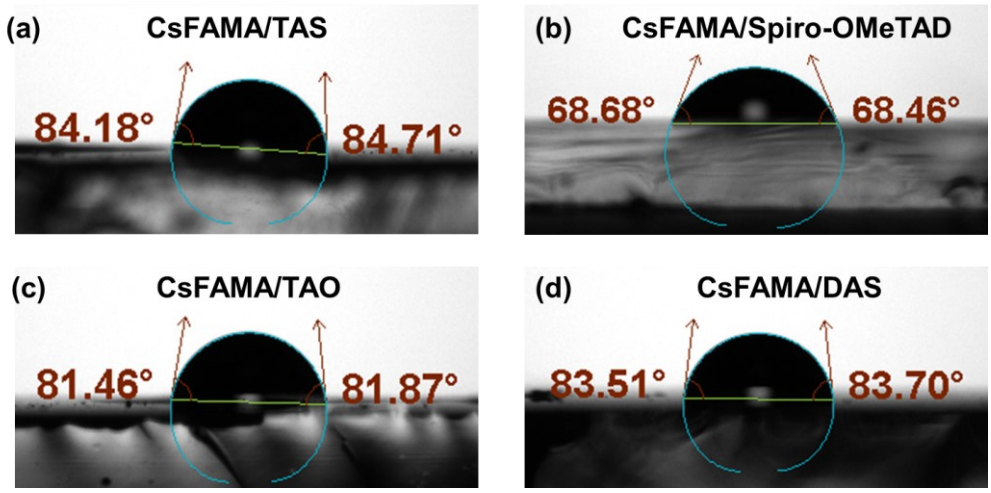

Figure 6. Water contact angles (CAs) for (a) TAS, (b) doped Spiro-OMeTAD, (c) TAO, and (d) DAS coated on perovskite films.

Furthermore, the morphology of aged perovskite films coated with HTMs after 100 days storage under ambient conditions was assessed by scanning electron microscopy (SEM) (**Figure S21**). All perovskite films coated with PTZ-HTMs show clear perovskite deposition with large grain size and homogeneous coverage, suggesting that the thin PTZ-HTMs (~65 nm) can still efficiently protect the underneath perovskite film upon the modified interface. On the other hand, the perovskite film coated with thick doped Spiro-OMeTAD (~120 nm, see **Figure S22**) exhibits a blurry effect with a sign of phase segregation, indicating a degradation for the perovskite film induced by hygroscopic dopants.[40] Contact-angle measurements were carried out to clarify the surface water resistance of the HTMs on perovskite films (see **Figure 6**). As summarized in **Table S14**, the water droplet contact angles on dopant-free PTZ-HTM films are reasonably larger than that on doped Spiro-OMeTAD film, since the dopants (e.g. tBP and LiTFSI) are mainly responsible for the high hygroscopicity of doped Spiro-OMeTAD layer. It is noteworthy that the difference of contact angles among those PTZ-HTMs is quite minor, further confirming that the high stability enhancement of TAS-based devices is achieved mainly by the interfacial modification induced by the Pb-S bond.

3. Conclusion

In summary, we present a simple yet effective strategy to synthesize a low-cost and dopant-free HTM based on phenothiazine, TAS, by introducing *N*,*N*-bis[4-(methylthio)phenyl]aniline functional group to modify the perovskite interface via the coordination of Pb-S bond. The results from DFT simulations show that the interfacial dipole moment driven by Pb-S bond enables the upward shift of CsFAMA perovskite work function when the HTM molecules vertically anchor to the surface of perovskite, contributing to an enhanced V_{oc} (>20 mV) in PSCs. Such a dipole moment also promotes the hole extraction, hinders the interfacial charge recombination, and contributes to the long-term device stability. We believe that our theoretical and experimental studies will provide a better understanding of the interfacial modification via sulfonated dopant-free HTM for achieving high-performance and stable *n-i-p* PSCs.

Supporting Information
Supporting Information is available from the Wiley Online Library or from the author.

Acknowledgements

R.L. and M.L. contributed equally to this work. R.L., C.W., Z.D., and H.Z. acknowledge the support from the Natural Science Foundation of China under Grant No. 21805151, Natural Science Foundation of Shandong Province, China under Grant No. ZR2018MB024, Young Taishan Scholars under Grant No. 201909120. M.L. acknowledges the Finnish Cultural Foundation (No. 00210670) for funding. P.V. acknowledges Jane and Aatos Erkko foundation (project 'ASPIRE'). S.P.R. acknowledges the financial support by the Australian government through the Australian Research Council (ARC) under the Centre of Excellence scheme (Project No. CE170100026), and NCI National Facility for computing resources. S.K.M thanks Dr. Jamie Booth for reading and providing useful feedback on the manuscript. This work is part of the Academy of Finland Flagship Programme, Photonics Research and Innovation (PREIN), Decision No. 320165.

Received: ((will be filled in by the editorial staff))
Revised: ((will be filled in by the editorial staff))
Published online: ((will be filled in by the editorial staff))

References

[1] J. P. Correa-Baena, A. Abate, M. Saliba, W. Tress, T. Jesper Jacobsson, M. Grätzel, A. Hagfeldt, *Energy Environ. Sci.* **2017**, *10*, 710.

[2] A. Kumar Jena, A. Kulkarni, T. Miyasaka, *Chem. Rev.* **2019**, *119*, 3036–3103.

[3] J. Y. Kim, J. W. Lee, H. S. Jung, H. Shin, N. G. Park, *Chem. Rev.* **2020**, *120*, 7867–7918.

[4] J. Jeong, M. Kim, J. Seo, H. Lu, P. Ahlawat, A. Mishra, Y. Yang, M. A. Hope, F. T. Eickemeyer, M. Kim, Y. J. Yoon, I. W. Choi, B. P. Darwich, S. J. Choi, Y. Jo, J. H. Lee, B. Walker, S. M. Zakeeruddin, L. Emsley, U. Rothlisberger, A. Hagfeldt, D. S. Kim, M. Grätzel, J. Y. Kim, *Nature* **2021**, *592*, 381.

[5] B. Chen, P. N. Rudd, S. Yang, Y. Yuan, J. Huang, *Chem. Soc. Rev.* **2019**, *48*, 3842–3867.

[6] H. Zhang, M. K. Nazeeruddin, W. C. H. Choy, *Adv. Mater.* **2019**, *31*, 1805702.

[7] L. M. Herz, *ACS Energy Lett.* **2017**, *2*, 1539–1548.

[8] T. Han, S. Tan, J. Xue, L. Meng, J. Lee, Y. Yang, *Adv. Mater.* **2019**, *31*, 1803515.

[9] W. H. Lee, C. Y. Chen, C. S. Li, S. Y. Hsiao, W. L. Tsai, M. J. Huang, C. H. Cheng, C. I. Wu, H. W. Lin, *Nano Energy* **2017**, *38*, 66.

[10] J. Lu, X. Lin, X. Jiao, T. Gengenbach, A. D. Scully, L. Jiang, B. Tan, J. Sun, B. Li, N. Pai, U. Bach, A. N. Simonov, Y. B. Cheng, *Energy Environ. Sci.* **2018**, *11*, 1880.

[11] L. Canil, T. Cramer, B. Fraboni, D. Ricciarelli, D. Meggiolaro, A. Singh, M. Liu, M. Rusu, C. M. Wolff, N. Phung, Q. Wang, D. Neher, T. Unold, P. Vivo, A. Gagliardi, F. De Angelis, A. Abate, *Energy Environ. Sci.* **2021**, *14*, 1429.

[12] X. Sun, F. Wu, C. Zhong, L. Zhu, Z. Li, *Chem. Sci.* **2019**, *10*, 6899.

[13] H. Lu, B. He, Y. Ji, Y. Shan, C. Zhong, J. Xu, J. LiuYang, F. Wu, L. Zhu, *Chem. Eng. J.* **2020**, *385*, 123976.

[14] H. Chen, W. Fu, C. Huang, Z. Zhang, S. Li, F. Ding, M. Shi, C.-Z. Li, A. K.-Y. Jen, H. Chen, *Adv. Energy Mater.* **2017**, *7*, 1700012.

[15] X. Yin, C. Wang, D. Zhao, N. Shrestha, C. R. Grice, L. Guan, Z. Song, C. Chen, C. Li, G. Chi, B. Zhou, J. Yu, Z. Zhang, R. J. Ellingson, J. Zhou, Y. Yan, W. Tang, *Nano Energy* **2018**, *51*, 680.

[16] F. Zhang, S. Wang, H. Zhu, X. Liu, H. Liu, X. Li, Y. Xiao, S. M. Zakeeruddin, *ACS Energy Lett.* **2018**, *21*, 48.

[17] X. Ding, C. Chen, L. Sun, H. Li, H. Chen, J. Su, H. Li, H. Li, L. Xu, M. Cheng, *J. Mater. Chem. A* **2019**, *7*, 9510.

[18] R. Li, Z. Dai, M. Zheng, C. Wang, Z. Deng, T. Zhuang, K. Feng, W. Yang, K. Yang, H. Zhang, *Macromol. Rapid Commun.* **2021**, *42*, 2000703.

[19] M. Saliba, S. Orlandi, T. Matsui, S. Aghazada, M. Cavazzini, J.-P. Correa-Baena, P. Gao, R. Scopelliti, E. Mosconi, K.-H. Dahmen, F. De Angelis, A. Abate, A. Hagfeldt, G. Pozzi, M. Graetzel, M. K. Nazeeruddin, *Nat. Energy* **2016**, *1*, 15017.

[20] X. Yin, L. Guan, J. Yu, D. Zhao, C. Wang, N. Shrestha, Y. Han, Q. An, J. Zhou, B. Zhou, Y. Yu, C. R. Grice, R. A. Awni, F. Zhang, J. Wang, R. J. Ellingson, Y. Yan, W. Tang, *Nano Energy* **2017**, *40*, 163.

[21] J. Salunke, X. Guo, Z. Lin, J. R. Vale, N. R. Candeias, M. Nyman, S. Dahlström, R. Österbacka, A. Priimagi, J. Chang, P. Vivo, *ACS Appl. Energy Mater.* **2019**, *2*, 3021.

[22] J. Zhang, Q. Sun, Q. Chen, Y. Wang, Y. Zhou, B. Song, N. Yuan, J. Ding, Y. Li, *Adv. Funct. Mater.* **2019**, *29*, 1900484.

[23] F. Zhang, X. Zhao, C. Yi, D. Bi, X. Bi, P. Wei, X. Liu, S. Wang, X. Li, S. M. Zakeeruddin, M. Grätzel, *Dye. Pigment.* **2017**, *136*, 273.

[24] F. Li, X. Deng, F. Qi, Z. Li, D. Liu, D. Shen, M. Qin, S. Wu, F. Lin, S. H. Jang, J.

Zhang, X. Lu, D. Lei, C. S. Lee, Z. Zhu, A. K. Y. Jen, *J. Am. Chem. Soc.* **2020**, *142*, 20134.

[25] H. Zhang, M. Liu, W. Yang, L. Judin, T. I. Hukka, A. Priimagi, Z. Deng, P. Vivo, *Adv. Mater. Interfaces* **2019**, *6*, 1901036.

[26] J. Xie, K. Yan, H. Zhu, G. Li, H. Wang, H. Zhu, P. Hang, S. Zhao, W. Guo, D. Ye, L. Shao, X. Guan, T. Ngai, X. Yu, J. Xu, *Sci. Bull.* **2020**, *65*, 1726.

[27] E. Zojer, T. C. Taucher, O. T. Hofmann, *Adv. Mater. Interfaces* **2019**, *6*, 1900581.

[28] M. Liu, M. Endo, A. Shimazaki, A. Wakamiya, Y. Tachibana, *ACS Appl. Energy Mater.* **2018**, *1*, 3722.

[29] S. Makuta, M. Liu, M. Endo, H. Nishimura, A. Wakamiya, Y. Tachibana, *Chem. Commun.* **2016**, *52*, 673.

[30] Y. Yamada, T. Nakamura, M. Endo, A. Wakamiya, Y. Kanemitsu, *J. Am. Chem. Soc.* **2014**, *136*, 11610.

[31] M. B. Johnston, L. M. Herz, *Acc. Chem. Res.* **2016**, *49*, 146.

[32] W. Li, X. Lai, F. Meng, G. Li, K. Wang, A. K. K. Kyaw, X. W. Sun, *Sol. Energy Mater. Sol. Cells* **2020**, *211*, 110527.

[33] Y. Wang, A. B. Djurišić, W. Chen, F. Liu, R. Cheng, S. P. Feng, A. M. Ching Ng, Z. He, *J. Phys. Energy* **2021**, *3*, 12004.

[34] X. Hu, H. Wang, M. Wang, Z. Zang, *Sol. Energy* **2020**, *206*, 816.

[35] Z. Li, J. Tinkham, P. Schulz, M. Yang, D. H. Kim, J. Berry, A. Sellinger, K. Zhu, *Adv. Energy Mater.* **2017**, *7*, 1601451.

[36] S. N. Habisreutinger, N. K. Noel, H. J. Snaith, *ACS Energy Lett.* **2018**, *3*, 2472.

[37] J. C. Brauer, Y. H. Lee, M. K. Nazeeruddin, N. Banerji, *J. Mater. Chem. C* **2016**, *4*, 5922.

[38] Z. Wang, Q. Lin, F. P. Chmiel, N. Sakai, L. M. Herz, H. J. Snaith, *Nat. Energy* **2017**, *2*, 17135.

[39] M. Saliba, M. Stolterfoht, C. M. Wolff, D. Neher, A. Abate, *Joule*, **2018**, 2, 1019–1024.

[40] M. Jeong, I. W. Choi, E. M. Go, Y. Cho, M. Kim, B. Lee, S. Jeong, Y. Jo, H. W. Choi, J. Lee, J. H. Bae, S. K. Kwak, D. S. Kim, C. Yang, *Science* **2020**, *369*, 1615.

The interaction between a sulfonated dopant-free hole transport material and perovskite via Pb-S bond induces a dipole moment that promotes hole extraction while hindering the interfacial charge recombination. The functionalization of perovskite surface upon the Pb-S bond enhances both device performance and stability of *n-i-p* standard perovskite solar cells.

R. L., M. L.,* S. K. M., A. H., Z. D., C. W., Z. D., S. P. R., P. V.,* H. Z.*

Sulfonated dopant-free hole-transport material promotes interfacial charge transfer dynamics for highly stable perovskite solar cells

ToC figure